The Netherlands Press

Journal of Airline Operations and Aviation Management

Article

AERODYNAMIC CHARACTERISTICS OF NACA 0012 AIRFOIL BY CFD ANALYSIS

Seshu Kumar Vandrangi

Doctoral Research Fellow,
Department of Mechanical Engineering,
Universiti Teknologi PETRONAS,
Persiaran UTP, 32610 Seri Iskandar, Perak, Malaysia

Orchid Id: https://orcid.org/0000-0002-5806-6913

E-mail: Seshu1353@gmail.com

Abstract.

The wind turbine's aerodynamic efficiency is heavily influenced by the aerodynamic airfoil blades. It's critical to choose the right aerofoil section for the blade. The angle of attack and its impact on lift and drag forces, such as high lift and low drag or vice versa, are key elements that determine the wind turbine system's efficiency. Using this as inspiration, the NACA 0012 airfoil profile is used to investigate the influence of angle of attack on the aerodynamic performance of wind turbine blades. The airfoil geometry is produced using computational fluid dynamics, according to the National Advisory Committee for Aeronautics (NACA) guidelines. The aerodynamic findings are evaluated in terms of static pressure and velocity distributions, as well as different angles of attack, in this study. The angle of attack increases as the lift/drag ratio decreases, according to the CFD study. Other elements, such as blade backflow turbulence and blade forces, should be addressed when evaluating the aerodynamic performance of NACA aerofoils.

Keywords: Aerodynamic efficiency, Reynolds Number, Turbulence, lift, Drag, Turbine, angle of attack.

Journal of Airline Operations and Aviation Management Volume 1 Issue 1
Received Date: 02 May 2022
Accepted Date: 06 June 2022
Published Date: 25 July 2022

1. Introduction

When fluid flows across an airfoil, it creates lift. Bernoulli's principle, Newton's third law of motion, or both effects might be the source of this lift. Because of the equal time argument, some of the scholars established that Bernoulli's principle is incorrect in these settings [1].

Because all particles must reach the tailing side at the same time, particles on the top level should travel a greater distance than rubbish on the lower floor. This indicates that, in accordance with Bernoulli's principle, there may be more tension at the bottom and considerably less stress at the top. Lift is caused by a change in pressure. The equal time argument is the name given to this particular argument [2]. Although the equal time argument is an excellent method to describe lift, it is incorrect. The first error occurs when two particles begin at the same point and travel to the tailing edge at the same time, covering different lengths of surface. In the two distinct streamlines, the Bernoulli's equation cannot be used. As a result, the equal time argument hypothesis fails to account for the lift force created by the aeroplane [3].

As the particles reach the air foil, they bend in the direction depicted in the diagram. If you look at the curve attentively, you'll see that the pinnacle of the particle may be under higher stress than the lowest, in order to provide the centrifugal force. The 'Coanda effect' occurs when a higher load drags the debris downward and the drift is always related to the airfoil. The go with the drift is also bent at the bottom of the airfoil. The bottom flow will be bent to a larger extent if the bottom surface is curved. The lift force is caused by this flow. The pressure decreases towards the airfoil at the top and increases towards the airfoil at the bottom. The lift is caused by the pressure differential. This is the explanation based on fluid mechanics [4].

Now we'll look at Newton's third law of motion. Because the deflection in the flow of air through the airfoil pulls the flow downward, according to Newton's third law, the air should also push in the opposite direction, resulting in the lift force[5].

The literature was examined for NACA airfoil types. Many researchers looked at the lift and drag characteristics of the NACA airfoil in general. Bhat et al. investigated the oscillation of NACA 0012 airfoils at low Reynolds numbers around the stall angle [6]. Benard et al. studied the use of a plasma actuator to improve the performance of air foils in both steady and unsteady scenarios [7].

Figure 1: Naca 0012 Airfoil[8]

2. CFD ANALYSIS OF NACA 0012 AIRFOIL:

For the purpose of analysing NACA airfoils. The NACA airfoil cross section geometry should be retrieved from the UIUC database, which provides all airfoil coordinates, and the coordinates of NACA 0012 should be taken from the database[9].

2.1. Geometry:

The data from the excel sheet is imported to the ansys workbench by choosing the coordinate files in the drawing tool, which loads the coordinates from the airfoil database.

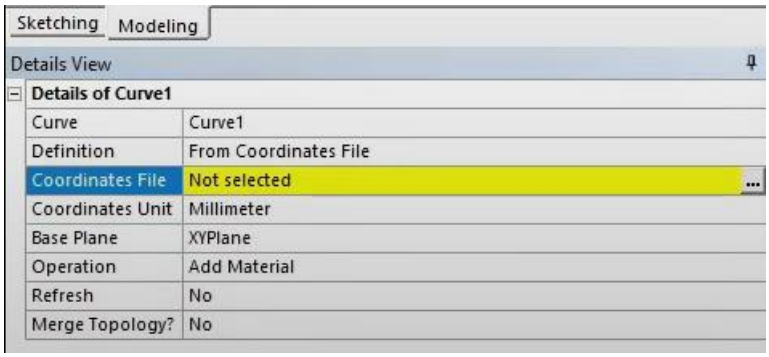

The coordinates should be set from the tip edge of the airfoil once the drawing is generated. A symmetrical line is formed using coordinates, and the geometry is constructed as indicated in the figure. The geometry must be ten times that of an airfoil. As a result, draw the lines as shown in the figure for height and length from the tip edge to the tailing edge.

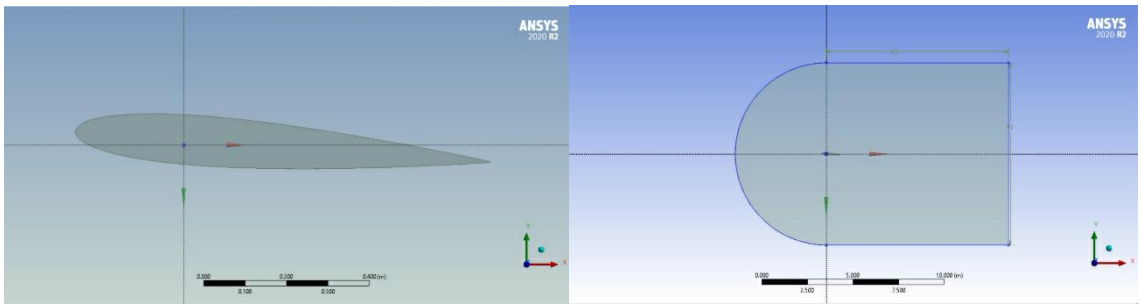

Figure 2: without and with enclosures of an airfoil

2.2. Mesh Generation:

The geometry is used to generate the mesh because the extended lines have already been drawn. The lines should be picked for edge sizing and the meshing behaviour is gentle, with the seven edges meshed with 250 equal divisions. After the edge meshing, all of the faces are selected to create a face meshing. With elements and nodes, the final mesh is constructed as shown in the picture. There is an airfoil wall for the named options, as well as intake velocity and outlet pressure.

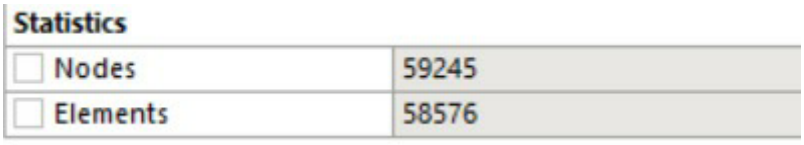

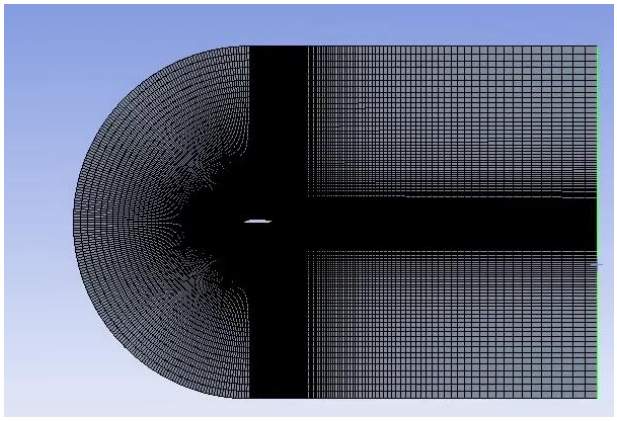

Figure 3: mesh generation

2.3. Setup:

The model is set to 2D, the CFD analysis resolution processes are set to 4, and the Double precision box should be ticked because single precision implies floating point values are represented in a 32-bit system, but double precision means they are represented in a 64-bit system. in 64-bit operating systems. As a result, calculations with double precision will be more precise. Though CPU performance suffers as a result of the longer solution time required to solve 64-bit floating-point values, the method also necessitates additional RAM to store those numbers. Because the flow is incompressible, the solution utilised for this issue is a pressure-based solver. When the flow is compressible, a density-based solver is employed. The time is in a steady state, and the velocity formulation is absolute. Planarity exists in 2D space.

For aerodynamic flows, the Spalart–Allmaras model was created. It isn't usually calibrated for typical business flows, and a few loose shear flows, particularly aircraft and spherical jet flows, cause much bigger errors. Furthermore, it is unreliable for predicting the decline of homogenous, isotropic turbulence. The fluid was air, with a density of 1.225 kg/m3 calculated from the mean sea level and a viscosity of 1.785x10-5 kg/m/s. Airfoil wall is the boundary condition. The velocity magnitude of the inlet is 43.9 m/s in the x-component direction. The turbulence intensity is 5% and the turbulent viscosity ratio is 10% in this case. The outlet pressure is in the absolute reference frame, with the gauge pressure set to 0 pascal and all other variables remaining constant.

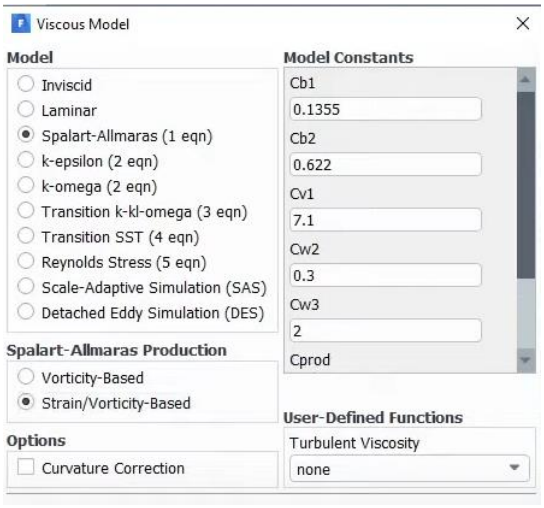

Figure 4: Viscous Model

The reference values may be found in the table below. This section will allow you to choose the technique for computing the variable parameters. In the Fluent, there are two forms of discretization: temporal and spatial. The former refers to the discretization of time-related concepts, while the latter refers to the discretization of space-related phrases. The pressure-based solver is linked the continuity and momentum equations to solve these equations, as mentioned in the previous chapter, therefore the Coupled scheme is employed in the Pressure-Velocity Coupling. The Pressure term is discretized spatially using the Body Force Weighted scheme, which is an optimal scheme for buoyancy driven flows. The Second Order Upwind technique is used to decrease the truncation error in the computation of Momentum, Turbulent Kinetic Energy, and Energy equations. Figure depicts the entire solution arrangement.

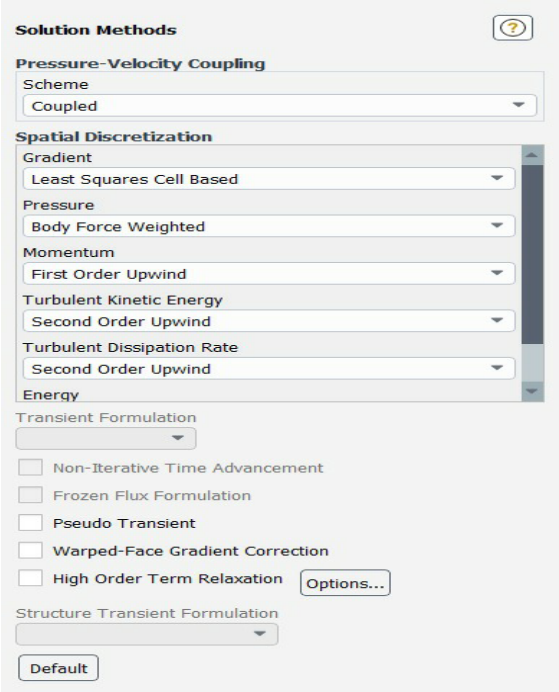

Figure 5: Solution Methods

The flow courant number for solution control is 200. When the duration is reduced, the fluid travels a shorter distance between time steps, which is the numerical stability number. The force report is necessary for the report definitions as lift and drag. Drag is measured in the X-direction, while lift is measured in the y-direction, both on the airfoil wall as cell zone conditions. The surface report is crucial.

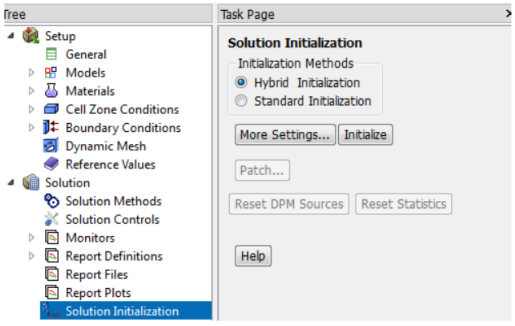

Figure 6: Solution Initialization

3. RESULTS AND DISCUSSIONS:

Surface pressure is used as a convergence criterion until it exceeds 1e-6. Initialization is a hybrid solution. The solution must be initialised using two methods once all of the preceding schemes have been set up. Standard or hybrid? As illustrated in Figure, the hybrid initialization is employed for steady state simulation for both pressure and density based solvers and improves the solution's convergence resilience. As a result, the same is employed in this investigation.

The residuals acquired by executing this for 1000 iterations are displayed in the image below. As the report definitions are supplied, the coefficient of lift and drag charts are generated. Lift is frequently reproducible because it is based on the Newtonian effect, which is easy to model. Newtonian effects are ethical, and they do not rely on viscous effects. The presence of viscous effects is caused by Navi Strokes, surface roughness, and a variety of other factors.

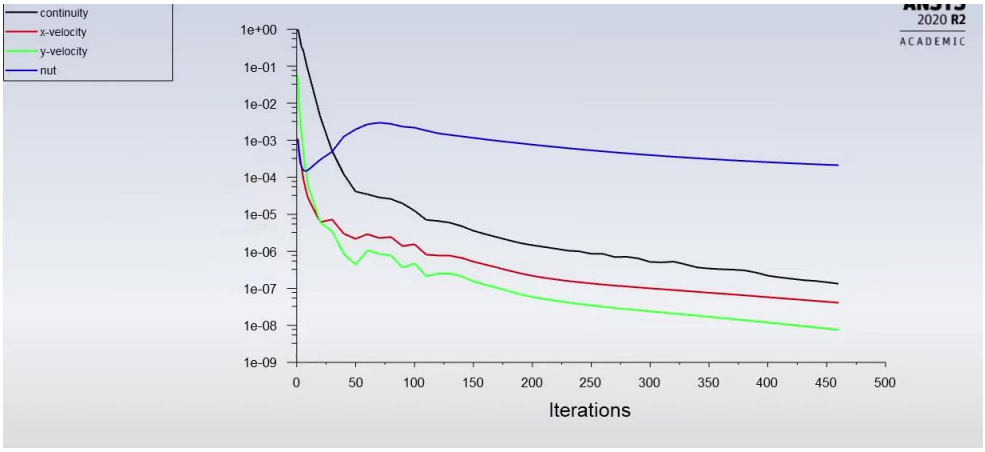

Figure 7: Residuals

The lift coefficient found is 0.423. The coefficient of lift has converged after 493 rounds. The coefficient of lift achieved at zero angle of attack is 0.423. The drag coefficient is 0.010 at the same number of iterations, according to the drag plot. So it may be done too well by employing the Spalart Allaramas model, and the simulation results can be carried further to velocity contours.

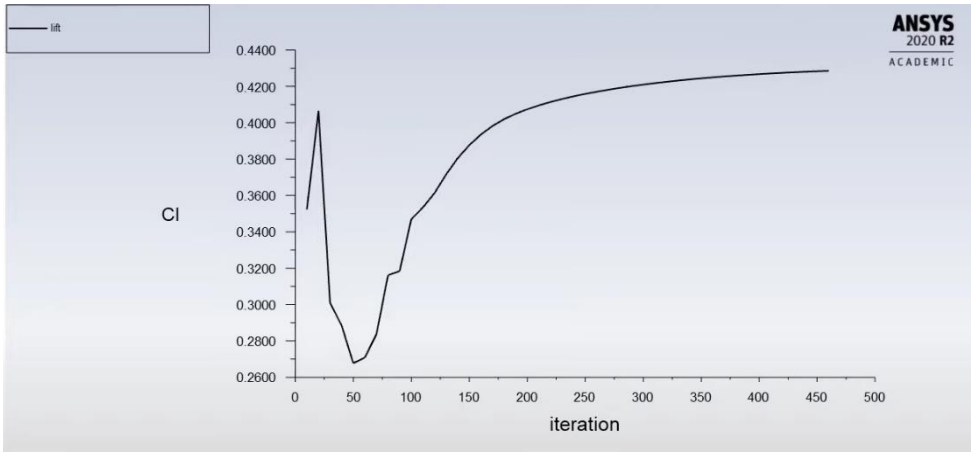

Figure 8: Coefficient of lift plot

The drag plot obtained differs from the lift plot by roughly 0.0042 at zero angle of attack. The length of the airfoil and the surface roughness have an impact on this. The drag plot is quite tough to produce right for the naca 0012, although the drag plots acquired were more accurate and matched the validation graphs very well[10].

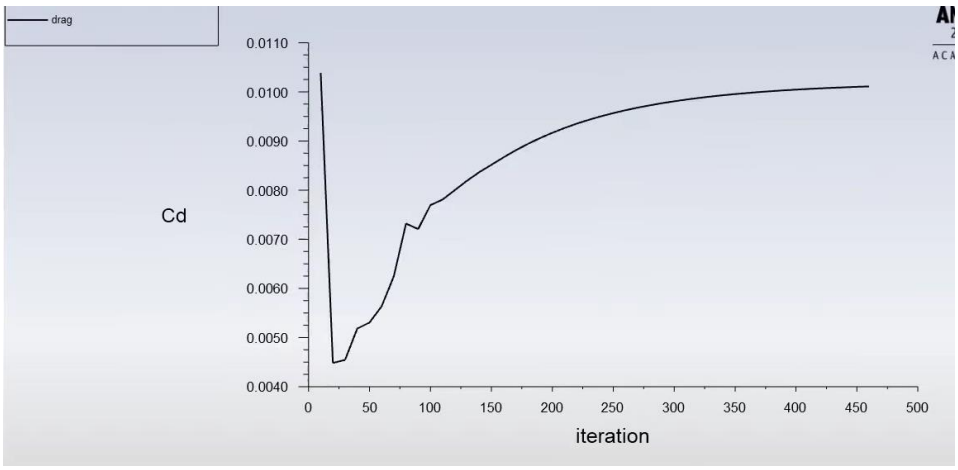

Figure 9: Coefficient of Drag Plot

The input velocity is provided as 13 degrees by looking at the velocity contour map, hence the coefficient of lift is 1.684 and the coefficient of drag is 0.028. At this simulation, the coefficients of lift and drag are calculated for each angle of attack. The top surface has a higher velocity than the lower surface, according to the contour.

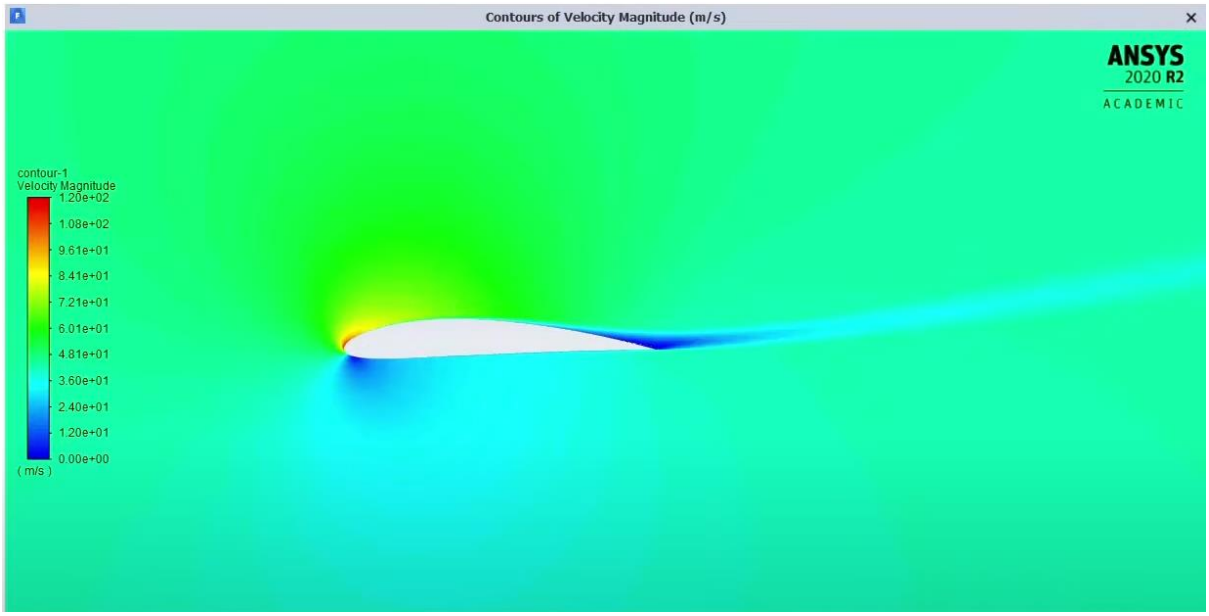

Figure 9: Velocity Contour

	Cl	()
airfoil		1.6841618
	Cd	()
airfoil		0.028005482

The pressure coefficient and the location of the airfoil are plotted, and the result is given in the figure below.

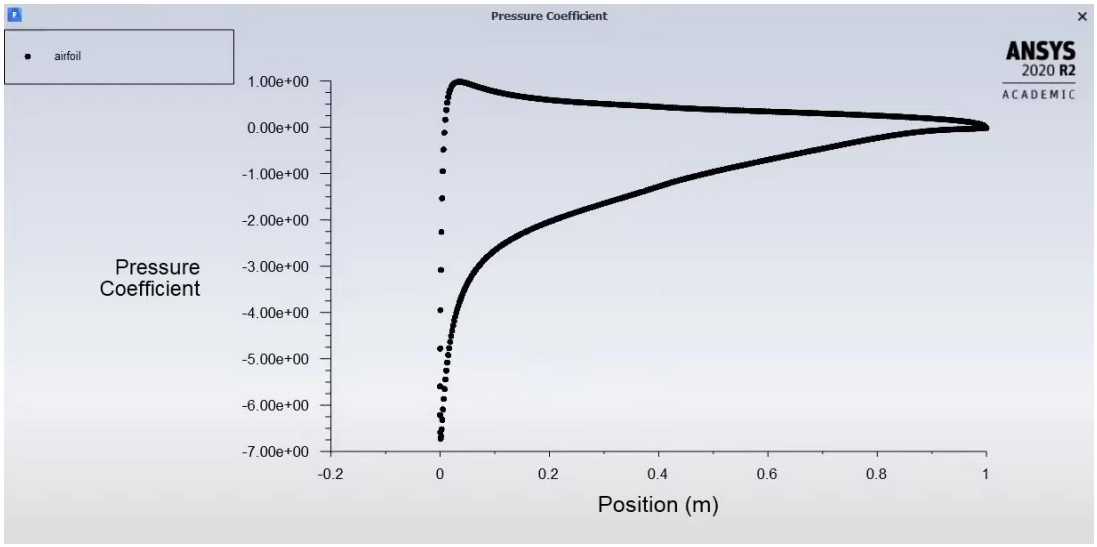

Figure 10: pressure coefficient vs position

4. CONCLUSION:

Drag and raise charts have coefficients that are similar to reference charts. The Coefficient of Lift graphic looks quite similar to NASA's 2D NACA 0012 Airfoil Validation Case[10], and the figures are nearly identical with minor changes. In addition, the graphs are completely converged when the procedure is terminated. The mesh high-quality of the profile improved as well. The coefficient of elevate increases with increasing attack angle, but only until the airfoil loses lift, according to the results. The Coefficient of Drag is determined by how close the angle of assault is to zero degrees, and because the angle of assault deviates far from zero degrees, the Coefficient of Drag decreases, the drag rises as the surface area of the airfoil restricting the flow increases.

References

[1] Jonathan Tompson, Kristofer Schlachter, Pablo Sprechmann, and Ken Perlin. Accelerating Eulerian Fluid Simulation With Convolutional Networks. arXiv, 2016.
[2] Julia Ling, Andrew Kurzawski, and Jeremy Templeton. Reynolds averaged turbulence modelling using deep neural networks with embedded invariance. Journal of Fluid Mechanics, 807:155–166, 2016.
[3] Brendan D. Tracey, Karthikeyan Duraisamy, and Juan J Alonso. A Machine Learning Strategy to Assist Turbulence Model Development. In 53rd AIAA Aerospace Sciences Meeting, pages 1–23, 2015.
[4] Andrea D. Beck, David G. Flad, and Claus-Dieter Munz. Deep Neural Networks for Data-Driven Turbulence Models. arXiv, 2018.
[5] Maziar Raissi, Paris Perdikaris, and George Em Karniadakis. Physics Informed Deep Learning (Part I): Data-driven Solutions of Nonlinear Partial Differential Equations. arXiv, pages 1–22, 2017.
[6] S. S. Bhat and R. N. Govardhan, "Stall flutter of NACA 0012 airfoil at low Reynolds numbers," Journal of Fluids and Structures, vol. 41, pp. 166-174, May 2013.
[7] N. Benard, J. Jolibois, and E. Moreau, "Lift and drag performances of an axisymmetric airfoil controlled by plasma actuator," Journal of Electrostatic, vol. 67, pp. 113-139, January 2009.
[8] Yousefi, Kianoosh and Reza Saleh. "Three-dimensional suction flow control and suction jet length optimization of NACA 0012 wing." Meccanica 50 (2015): 1481-1494.
[9] "UIUC Airfoil Data Site," UIUC Airfoil Data Site. https://mselig.ae.illinois.edu/ads/coord_database.html (accessed Jun. 11, 2022).
[10] "Turbulence Modeling Resource." https://turbmodels.larc.nasa.gov/naca0012_val.html (accessed Jun. 11, 2022).